The supramolecular organization of self-assembling chlorosomal bacteriochlorophyll *c*, *d*, or *e* mimics

Tobias Jochum*†, Chilla Malla Reddy†‡, Andreas Eichhöfer‡, Gernot Buth*, Jędrzej Szmytkowski§¶, Heinz Kalt§¶, David Moss*, and Teodor Silviu Balaban‡¶‖

*Institute for Synchrotron Radiation, Karlsruhe Institute of Technology, Forschungszentrum Karlsruhe, Postfach 3640, D-76021 Karlsruhe, Germany; ‡Institute for Nanotechnology, Karlsruhe Institute of Technology, Forschungszentrum Karlsruhe, Postfach 3640, D-76021 Karlsruhe, Germany; §Institute of Applied Physics, Karlsruhe Institute of Technology, Universität Karlsruhe (TH), D-76131 Karslruhe, Germany; and ¶Center for Functional Nanostructures, Universität Karlsruhe (TH), D-76131 Karslruhe, Germany

Edited by James R. Norris, University of Chicago, Chicago, IL, and accepted by the Editorial Board July 18, 2008 (received for review March 22, 2008)

Bacteriochlorophylls (BChls) *c*, *d*, and *e* are the main light-harvesting pigments of green photosynthetic bacteria that self-assemble into nanostructures within the chlorosomes forming the most efficient antennas of photosynthetic organisms. All previous models of the chlorosomal antennae, which are quite controversially discussed because no single crystals could be grown so far from these organelles, involve a strong hydrogen-bonding interaction between the 3^1 hydroxyl group and the 13^1 carbonyl group. We have synthesized different self-assemblies of BChl *c* mimics having the same functional groups as the natural counterparts, that is, a hydroxyethyl substituent, a carbonyl group and a divalent metal atom ligated by a tetrapyrrole. These artificial BChl mimics have been shown by single crystal x-ray diffraction to form extended stacks that are packed by hydrophobic interactions and in the absence of hydrogen bonding. Time-resolved photoluminescence proves the ordered nature of the self-assembled stacks. FT-IR spectra show that on self-assembly the carbonyl frequency is shifted by ≈30 cm^{-1} to lower wavenumbers. From the FT-IR data we can infer the proximal interactions between the BChls in the chlorosomes consistent with a single crystal x-ray structure that shows a weak electrostatic interaction between carbonyl groups and the central zinc atom.

chlorosome model | crystal structure | FT-IR | light-harvesting | time-resolved fluorescence

Green photosynthetic bacteria appeared some three billion years ago in an anoxic atmosphere. To adapt to specific illumination conditions, the green sulfur bacteria (*Chlorobiaceae*) and the phylogenetically quite distant gliding filamentous bacteria (*Chloroflexaceae*) have evolved a special light-harvesting organelle that agglomerates bacteriochlorophylls (BChls) *c*, *d*, or *e* (Fig. 1) as the main antenna pigments (1–3). Because of the dense packing of green BChls, as revealed by early electron microscopy studies (4–6), these organelles that are attached to the inner side of the cytoplastic membrane were called "chlorosomes" to reflect their "green sac" nature. Some brown bacterial species also have well developed chlorosomes (7). An aerobic phototroph having chlorosomes and belonging to the phylum *Acidobacteria* was discovered recently in hot springs (8). By scavenging photons at great depths, chlorosomal expressing bacteria thrive where other forms of life cannot rely on photosynthesis. In the Black Sea, for example, a *Chlorobium* species that contains BChl *e* was identified as much as 100 m under the water surface (9). Astonishingly, a BChl *c*-containing microbe has recently been found at a depth of 2,390 m, close to a volcanic vent in the Pacific Ocean, showing that chlorosomes enable photosynthesis with near-infrared wavelengths even in the absence of solar radiation (10).

Very recent high-resolution images confirm that chlorosomes are flattened cigar-shaped nanostructures with dimensions of ≈20 × 50 × 200 nm (7, 11). Their size varies depending on the organism and illumination conditions of the habitat. Despite more than three decades of research efforts, in the absence of direct structural evidence from x-ray single crystal structures, the exact nature of BChl superstructures remain elusive and these have been controversially discussed in the literature (1–3, 7, 11–17). It is now generally accepted that the main feature of chlorosomes is the self-assembly of BChls and that these pigments are not bound by a rigid protein matrix as is the case of other, well characterized light-harvesting systems (1). Small-angle x-ray scattering (SAXS) experiments combined with transmission electron microscopy (TEM) and cryo-TEM both on green bacterial chlorosomes from *Chlorobium tepidum* (11, 12) and brown bacterial chlorosomes from *Chlorobium phaeovibroides* (7) and *Chlorobium phaeobacterioides* (7) have indicated a lamellar structure of the BChl assemblies. The data could not be reconciled with an earlier proposed cylindrical model (13, 14) and this has now rekindled the discussion on the true chlorosome architecture. The SAXS data show sharp reflexes with ≈2-nm spacings and these are assumed to represent Mg–Mg distances. However, in these more recent models hydrogen bonding was still assumed to occur between dimers (7, 12). Another very recent study by solid-state NMR on ^{13}C-labeled chlorosomes has discussed all previous models and favors a parallel hydrogen-bonded dimer model as the most probable one (15, 16). Molecular mechanics calculations and exciton theory have been applied in a very thorough theoretical investigation on the different possible geometries such as tube, lamella, or spiral-type for the chlorosomal aggregates (17).

Understanding the exact architecture of the chlorosomes is not only an important biological research goal but also this would allow replication of the light-harvesting ability with fully synthetic pigments in photovoltaic devices for biomimetic energy transduction. The self-assembly algorithm programmed within chlorosomes could be reproduced with completely artificial pigments (18–22), that lends hope that it can be used in solid-state devices such as hybrid solar cells (23, 24). This would enable efficient light capturing and operation also under low-light illumination conditions. Such an optimal photon management is not possible with the present, state-of-the-art solar cells. Our synthetic BChl *c*, *d*, or *e* mimics (Fig. 1) have the advantages

Author contributions: T.S.B. designed research; T.J., C.M.R., A.E., J.S., D.M., and T.S.B. performed research; G.B., H.K., and D.M. contributed new reagents/analytic tools; T.J., A.E., J.S., D.M., and T.S.B. analyzed data; T.S.B. wrote the paper; G.B. built the Small Crystal Diffractometry (SCD) beamline at the ANKA Synchrotron; and H.K. supervised the time-resolved fluorescence measurements and built the set-up.

The authors declare no conflict of interest.

This article is a PNAS Direct Submission. J.R.N. is a guest editor invited by the Editorial Board.

Data deposition: The atomic coordinates have been deposited in the Cambridge Crystallographic Data Center (ID code CCDC-677194).

†T.J. and C.M.R. contributed equally to this work.

‖To whom correspondence should be addressed. E-mail: silviu.balaban@int.fzk.de.

This article contains supporting information online at www.pnas.org/cgi/content/full/0802719105/DCSupplemental.

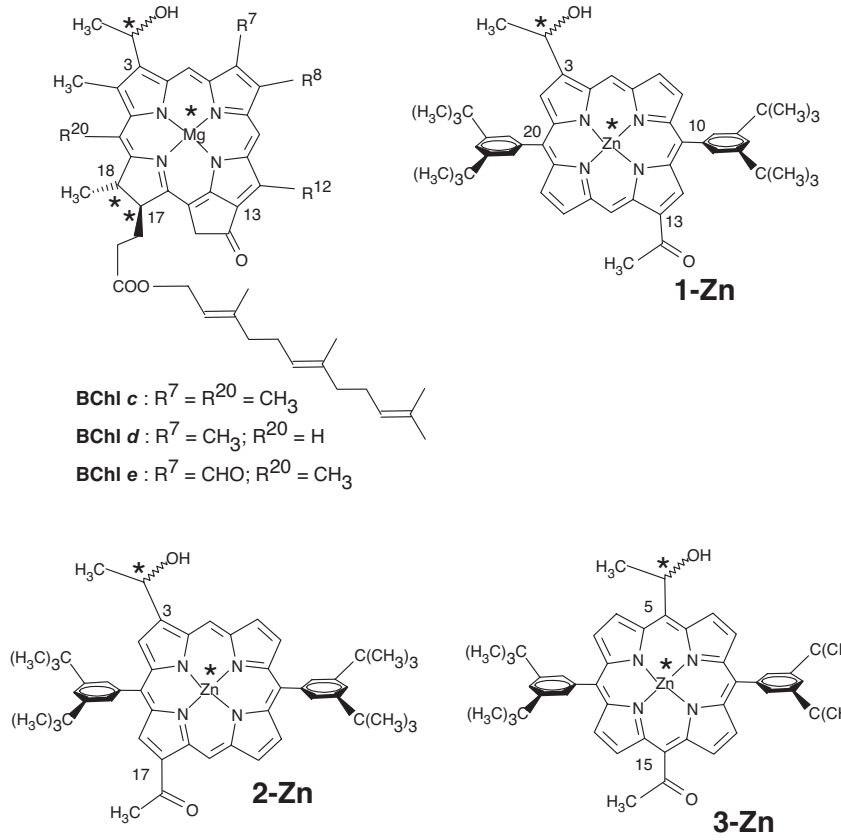

Fig. 1. Naturally occurring BChls and their synthetic porphyrinic mimics. In BChls R^8 and R^{12} can be different homologous groups such as methyl, ethyl, *n*-propyl, or isobutyl. Farnesol is depicted as the long-chain alcohol esterifying the 17-propionic acid but also other fatty alcohols such as stearol, cetol, phytol, geranyl-geraniol, etc., can be encountered in various bacteria. Metal-centered asterisks denote stereocenters formed on ligation. The atom numbering of porphyrins deliberately follows that of BChls.

that they are readily available without the need of culturing bacteria and are chemically more stable.

In the present study we have examined the Fourier transform infrared (FT-IR) spectra of self-assemblies from synthetic BChl models possessing a hydroxyethyl group in the northern half of the porphyrin molecule and an acetyl recognition group in the southern half. To investigate the importance of hydrogen bonding and metal ligation, additional compounds lacking either a hydroxyl group (**4-Zn**–**6-Zn**, **4-Mg,** and **5-Mg**) or the metal atom (**1-FB**–**3-FB**) were also studied (Fig. 2). Zinc as the central metal atom leads to more stable assemblies than magnesium. Zinc has similar coordination properties and also occurs naturally in photosynthetic bacteria adapted to an acidic environment (pH 3.5), in which a magnesium atom would inevitably be replaced by hydrogens leading to the corresponding free base (*25*).

The 3^1-carbon atom of the hydroxyethyl group is a stereocenter (asterisks in Fig. 1) that generates two enantiomorphic porphyrins. We have used the racemic mixture because the separated enantiomers self-assemble less readily (21). It thus appears that the heterochiral self-assembly is thermodynamically favored compared with a homochiral mechanism. This explains why in the chlorosomes both 3^1-epimers of BChls are encountered, which was a long-standing question because, in natural systems, enantiopure compounds are usually the outcome of enzymatic biosyntheses.

The BChl mimics **1-Zn**–**6-Zn** self-assemble in nonpolar solvents such as dry *n*-heptane or cyclohexane. Depending on the anchoring positions of the hydroxyethyl and/or acetyl recognition groups, red-shifted and broadened visible absorption maxima are diagnostic for the self-assemblies. Monomeric forms are obtained in zinc-coordinating solvents such as dry tetrahydro-

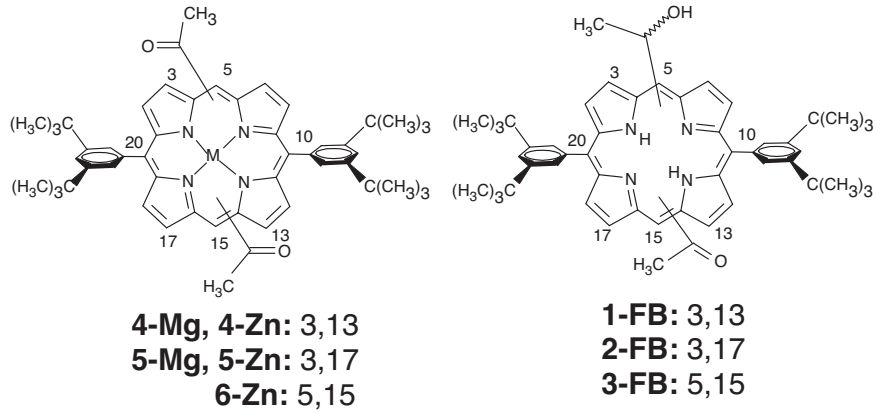

Fig. 2. Zinc and magnesium complexes of diacetyl porphyrins which self-assemble in the absence of hydroxyl groups (*Left*) and the free bases (FB) as control compounds exhibiting no self-assembly (*Right*). The numbers following the semicolon indicate anchoring positions of the recognition groups on the macrocycle, northern half first.

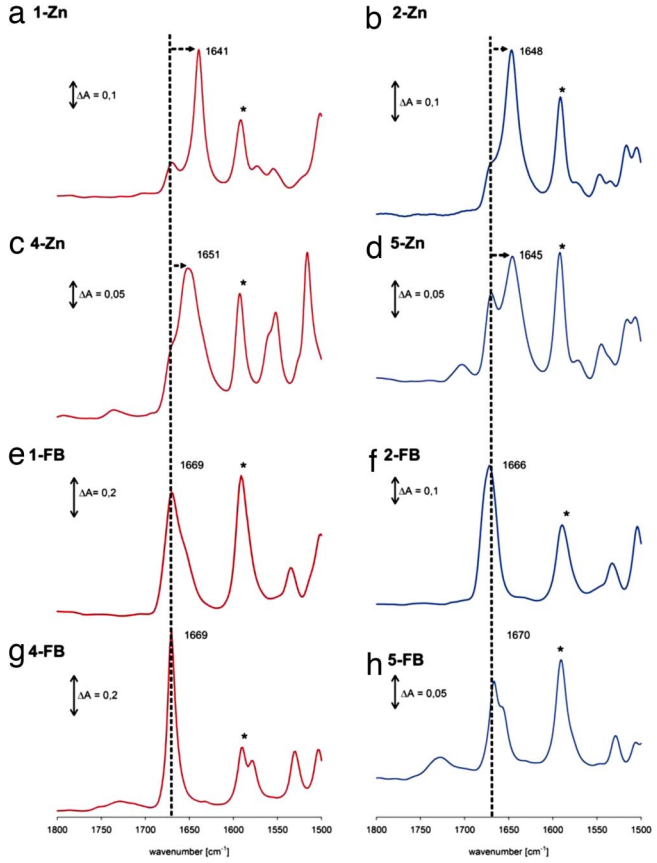

Fig. 3. FT-IR spectra as KBr pellets of various zinc BChl mimics and comparison with the free bases. Red traces are of 3,13-substituted compounds and blue traces are from the isomeric 3,17-compounds. The asterisk denotes the porphyrin-breathing mode ≈1,592 cm^{-1} which serves as a marker band making thus clear shifts of the $\nu_{C=O}$ indicated by the arrows from the dotted lines.

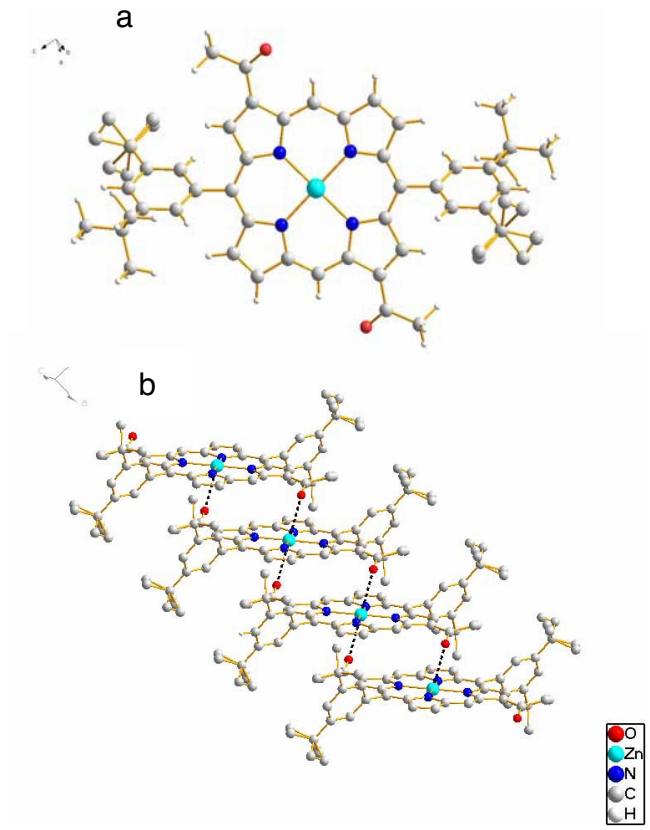

Fig. 4. Single-crystal X-ray structure of **4-Zn**. (*a*) Monomer of **4-Zn**. (*b*) Stack of **4-Zn** with hydrogen atoms omitted for clarity. Tertiary butyl groups are partially disordered over two different conformations.

furan (THF). In the FT-IR spectra, the regions of interest are the carbonyl stretching region (1,800–1,500 cm^{-1}) and the hydroxyl deformation regions (3,500–3,000 cm^{-1}) and from the infrared band shifts in the self-assemblies compared with the monomers, one can precisely determine which functional groups participate in supramolecular interactions. Typical FT-IR spectra recorded in KBr pellets are shown in Fig. 3. The KBr does not affect the spectra as judged from KBr-free spectra recorded from powder samples [supporting information (SI) Fig. S1]. The free acetyl group in compounds **1-Zn** and **2-Zn** is in conjugation with the porphyrin skeleton and has its $\nu_{C=O}$ at ≈1,670 cm^{-1}, as shown by the spectra of the free bases and the spectra recorded in solution in THF, which prevents self-assembly. In contrast, in the nonpolar solvent cyclohexane and in the KBr pellets, the vibrational frequency of the acetyl group is strongly shifted to lower wavenumbers by 30 cm^{-1} in the case of **1-Zn** and by 24 cm^{-1} in the case of **2-Zn** (Fig. S2). The porphyrin breathing mode appears in all zinc complexes at 1,592 cm^{-1} and it serves as a marker band so that the shifts of the carbonyl band are clearly visible.

In **3-Zn** the *meso* 15-acetyl group is not in conjugation with the π-macrocyle because of steric hindrance with the neighboring β-pyrrolic hydrogens and, in this case, the $\nu_{C=O}$ is at ≈1,685 cm^{-1}. The behavior of the diacetylated zinc porphyrins **4-Zn**–**6-Zn** can be similarly understood. In THF solution the monomer carbonyl frequency appears again at 1,670 cm^{-1} for **4-Zn** and **5-Zn**. In cyclohexane and in KBr pellets these zinc complexes show self-organization despite the absence of a hydroxyl group capable of hydrogen bonding. This is evident from the large shift of $\nu_{C=O}$ to ≈1,650 cm^{-1}, which is a clear indication that the zinc atom is interacting with the acetyl groups in neighboring stacking porphyrins. In all cases a residual shoulder stemming from monomeric forms is also visible at 1,670 cm^{-1}, indicative of the coexistence of free acetyl groups with ones interacting with zinc atoms. The magnesium counterparts **4-Mg** and **5-Mg** behave very similarly except that the contribution of monomers at 1,666 cm^{-1} is now larger (Fig. S3).

The large shift of $\nu_{C=O}$ on self-assembly is indicative of an electrostatic interaction of the carbonyl group with the zinc atom in a closely stacked porphyrin. A putative O-H–O=C< hydrogen bond, which could also donate electron density from the carbonyl group, thus lowering its frequency, would lead to smaller $\Delta\nu_{C=O}$ shifts (On hydrogen bonding in solution, shifts for $\nu_{C=O}$ of 10–12 cm^{-1} have been described for various aromatic ketones. For a review, see ref. 26.)

We could confirm that the Zn–O=C< electrostatic interaction is indeed encountered by solving a single-crystal x-ray structure of **4-Zn**. The crystals of **4-Zn** were of sufficient size so that normal data collection, structure solving, and refinement by direct methods could be used. Under identical conditions, **Zn-5** as well as **Mg-4** and **Mg-5** gave only very thin needles, which needed synchrotron radiation for obtaining preliminary datasets that could not yet be refined satisfactorily. Fig. 4 shows the molecular structure and the main supramolecular interactions of **4-Zn**.

In **4-Zn** the two acetyl groups are on the main diagonal passing through the zinc atom, just as the 3 and 13^1-recognition groups are in the BChls. Within a monomer an *anti* orientation of the carbonyl groups is encountered, which is the more favorable conformation because of a minimization of the dipole moment. Extended stacks in a staircase arrangement are formed by π–π

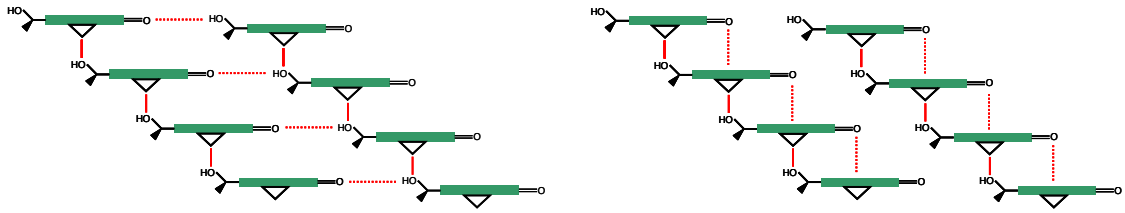

Fig. 5. Models derived from the FT-IR and NMR data for BChls. (*Left*) Previous models (13, 14, 27, 30). (*Right*) Newly proposed supramolecular interactions leading to a paradigm shift in the interpretation of the large displacement to lower wavenumbers of the $\nu_{C=O}$ due to the weak zinc ligation instead of a strong hydrogen bonding network depicted at *Left*. Because the stacks are decoupled, they can pack in different orientations solely by hydrophobic interactions.

interactions combined with a weak >C=O–Zn electrostatic interaction between adjacent monomers. This is not a typical coordinative bond because the O–Zn distance is >2.8 Å long and the oxygen lone pairs are not pointing toward the Zn. Interestingly, the acetyl group is almost coplanar with the porphyrin macrocycle, the C2-C3-C3^1-O dihedral being +10°. A much stronger interaction could have been achieved by twisting the acetyl group out of conjugation. That this is not the case shows that the dominant interaction is π-stacking. The stacks of **4-Zn** pack tightly by solely hydrophobic interactions.

Within BChls the annulated cyclopentanonic ring ensures more or less the same coplanar conformation of the 13^1 carbonyl group allowing for a similar recessive >C=O–Mg electrostatic interaction. FT-IR spectra of BChls show a similar large shift of the $\nu_{C=O}$ to ≈1,645 cm^{-1} (27). This allows us to draw an unprecedented analogy between our synthetic mimics and the chlorosomal BChl self-assemblies. The large shift to lower wavenumbers that occurs on self-assembly of BChls has been previously interpreted as due to an exceptionally strong hydrogen-bonding interaction (27). In two crystal structures of **3-Zn** (21, 22), despite the presence of a hydroxyethyl group, no hydrogen bonding is possible because of the weak electrostatic interaction between the acetyl groups and the central zinc atom in a neighboring porphyrin that is π-stacked. Very recently, Lindsey and coworkers, after designing synthetic methods for one-carbon-atom-based recognition groups for porphyrins, have also shown the absence of putative hydrogen bonds with formation of staircase architectures (28). Formation of extended stacks in BChls is in accord with previous solid-state ^{13}C-NMR data (29–31) and this is depicted in diagrams in Fig. 5. The fact that stacks are not hydrogen-bonded allows for hydrophobic and dispersive forces to dominate in gluing stacks together. Because these interactions are not directional, dense packing can be assured in various orientations allowing for considerable disorder. Either up-running stacks or down-running stacks can form extended domains, which have been imaged by TEM (7, 11, 12). This disorder was also seen in the solid-state NMR work as splittings of several signals (14–16, 31) but was interpreted as two concentrically cylindrical assemblies of BChls (14). The recent SAXS data are incompatible with any form of rod-like assemblies. Rather, a lamella-like stacking is encountered and, based on our previous x-ray structures (21) and present FT-IR data, we propose that the stacks are packed by hydrophobic interactions alone. Very recently, an elegant mutagenesis study on knockout mutants from *Chlorobium tepidum* involving inhibition of carotenoid biosynthesis shows that the carotenoids are also packed by hydrophobic interactions within self-organized BChls (32). Fig. 6 presents our model for BChl self-assemblies that fulfils all spectroscopic data gathered so far on the natural systems and on the synthetic mimics, which include two crystal structures and the present FT-IR data. We exclude that dimers serve as the building block on the basis of our crystal structures where extended stacks with the same 5½ coordination of zinc atoms was encountered. This asymmetric six-coordination had actually been proposed earlier by Blankenship and collaborators (33, 34) but later abandoned on the basis of FT-IR and resonance Raman studies that seem to indicate pentacoordination. The fact that the >C=O–Mg distance is very long in our model (3.3 Å) reconciles these analyses, which are actually dominated by the strong Mg–OH ligation.

That chlorosomes are the most efficient natural antenna systems is undisputed. Their detailed supramolecular architecture is controversial, and so is the fact that we can extrapolate the detailed structural evidence gained on our Zn- and Mg-containing self-assembled mimics to the BChls, which have different peripheral substituents. That the fluorescence is not quenched on self-assembly, neither in the chlorosomes, nor in our mimics, is a strong indication of a similar arrangement of the chromophores. Time-resolved fluorescence spectroscopy allows a clear differentiation of the decays due to the monomers (τ_1 = 1.5–2 ns) and to the self-assembled species (τ_2 = 40–100 ps). Selective excitation can be performed as shown in Fig. 7. The decays are monoexponential in Fig. 7 *Upper Left Inset*, and biexponential in the other three insets.

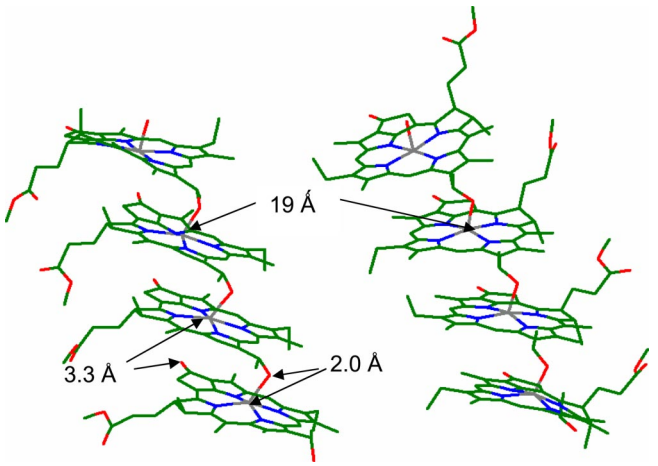

Fig. 6. Model of the proximal interactions in the chlorosome. The x-ray coordinates for **3-Zn** and **4-Zn** served as initial basis for geometry optimizations by using the structure of BChl *c* generated within the HyperChem Package 7.5. Two parallel running stacks of BChl *c* are presented as tetramers with ≈1.9-nm spacing between Mg atoms. The magnesium atom (gray) has a 5½ coordination: 4 from the tetrapyrrolic nitrogens (blue), a strong 2.0-Å ligation from the oxygen atom (red) of the 3-hydroxyethyl group, and a weak ligation from the 13^1-carbonyl group with a length of ≈3.3 Å. Two diastereomeric configurations are shown: the magnesium atoms are α-ligated (*Left*), whereas, at the more unfavorable configuration, β-ligation is shown (*Right*) (for the α/β dichotomy, see ref. 35). This ensures considerable heterogeneity to BChl self-assemblies and additional disorder is induced by the long-chain alcohol esterifying the 17-propionic acid residue, which can interdigitate in multiple conformations (in the model above, only a methyl group is shown). In addition to the magnesium ligations, multiple weak hydrophobic interactions, also with carotenoids, are thus alone responsible for the supramolecular self-organization of the chlorosome pigments.

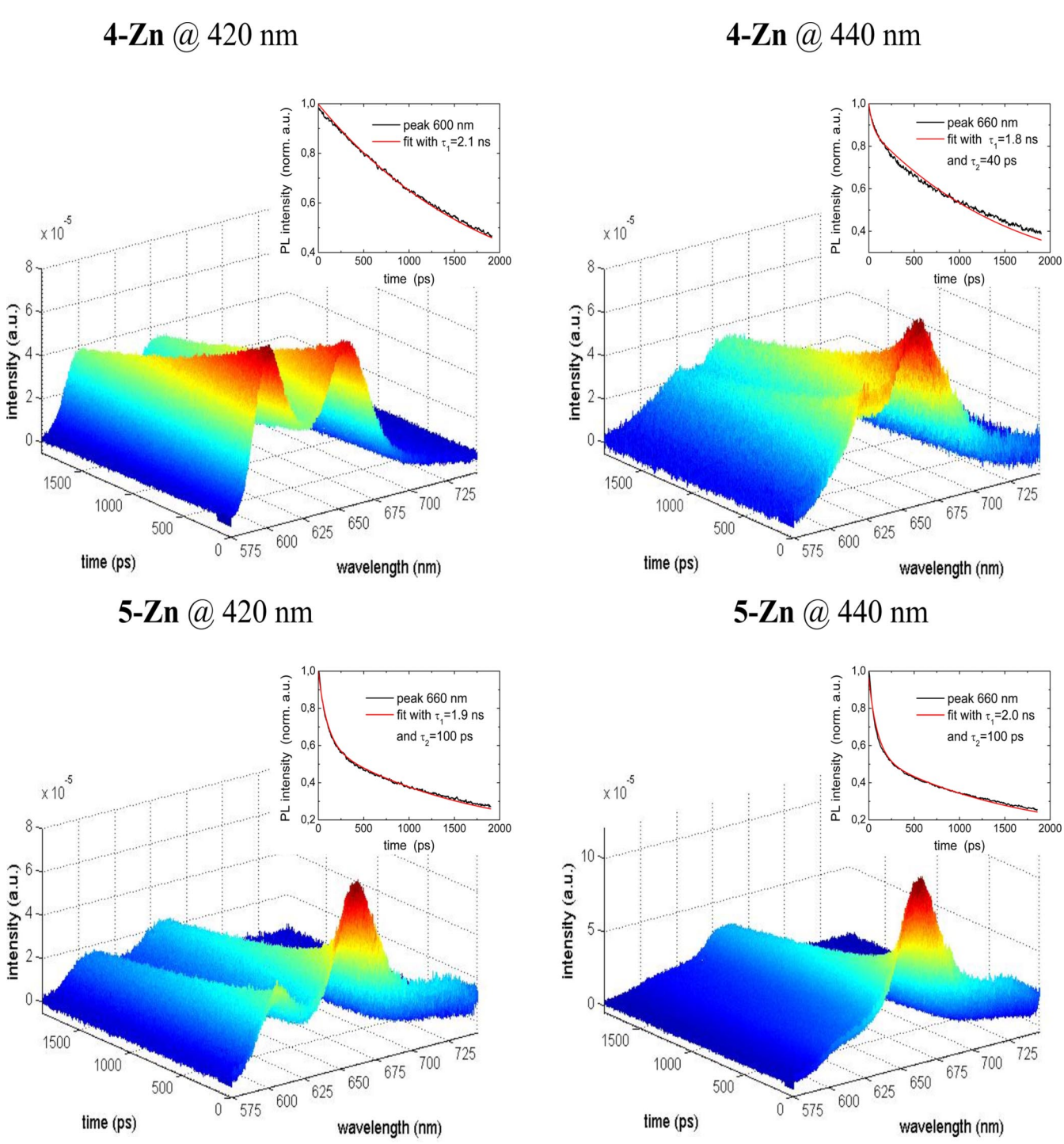

Fig. 7. Color-coded, time-resolved fluorescence decays after selective excitation of monomeric (at 420 nm) or of the self-organized species (at 440 nm).

Usually randomly oriented chromophores in an aggregated state self-quench their fluorescence making their application as light harvesters in solar cells problematic. Artificial self-assembling chromophores, which mimic the chlorosomal BChls, do not have this disadvantage and are good candidates for incorporation into hybrid solar cells (23, 24).

The chlorosomal BChls act collectively and rapidly transfer the excitation energy to a trimeric BChl *a*-containing protein, the Fenna–Matthews–Olson (FMO) protein situated in a baseplate close to the reaction center which is embedded within the membrane. Excitation energy transfer within the aggregates occurs on the 100-fs timescale with a 1- to 2-ps component that can be attributed to interstack transfers, while trapping within the FMO occurs on the 35- to 50-ps timescale (36). Although our setup cannot resolve the ultrafast energy transfer components, the investigated self-assembled mimics have potentially an adequate lifetime (40–100 ps) for the radiant energy to be efficiently trapped within an artificial reaction center. The possibility to act as an antenna is given by the large photon capture cross-section of assemblies on the 100-nm to 1-μm scale, so that once a chromophore is excited, the photon energy is efficiently and rapidly transferred without annihilation so that it can be trapped eventually. Additionally, the

absorption spectra are considerably broadened so that a large wavelength range of the solar radiation can be tapped. The spectral and kinetic inhomogeneity encountered in the chlorosomes and the broadened Q_y transition, as the recent theoretical study indicates (17), could be due to "a variety of BChl-aggregate structures" comprised of upward and downward stacks with 5½ coordinated magnesium atoms in an asymmetric fashion.

In conclusion, we have proposed, based on FT-IR studies of synthetic BChl mimics for which single-crystal structural data were also gained, a model for the self-organization of pigments within chlorosomes. This model is compatible with all previous experimental data and reconciles various analyses. By understanding the details of natural photosynthesis it is hoped to replicate in artificial, man-made devices light-harvesting and subsequent photoinduced charge separation to convert and store efficiently solar energy into useful energy.

Materials and Methods

The BChl mimics **1-Zn**–**6-Zn** were synthesized as described in ref. 18. FT-IR spectra were recorded under identical conditions by using prolonged purging of the instrument (Bruker Equinox 55) with dry nitrogen and long accumulation times (1,024 scans). Consistent and reproducible results could be obtained if the KBr and solvents used were thoroughly dried. Pellets of KBr were prepared from powder that which had been self-assembled in dry *n*-heptane or cyclohexane, centrifuged, and thoroughly dried overnight in vacuum (10^{-2} bar). For spectra in solution and for powder samples in the absence of KBr see the *SI Text*. For the powder samples we used a Bruker IRScope II microscope attached to a Bruker 66 v/s FTIR spectrophotometer, equipped with a liquid-nitrogen-cooled MCT detector. The powder sample was compressed between two 1-mm CaF_2 windows, then the windows were separated and the material adhering to the window was measured, selecting an area where the microscope's field of view was completely filled by the material and the thickness of the film was suitable for good signals with neither excessively high nor excessively low absorbance. Spectra obtained from different areas were identical, indicating no homogeneity issues. These were transmission measurements through the 36× objective.

4-Zn and **5-Zn** were prepared from the corresponding free bases by metallation with anhydrous zinc acetate in a chloroform/methanol (4:1, vol/vol) mixture. **4-Mg** and **5-Mg** were similarly prepared from their free bases by the method of Lindsey (37) by using $MgBr_2$ $O(Et)_2$ in dichloromethane freshly distilled from calcium hydride.

Slow evaporation of a saturated solution of **4-Zn** in dry dichloromethane, which was diluted with twice its volume with dry *n*-heptane, yielded in well formed crystals. Single-crystal x-ray diffraction data of **4-Zn** were collected by using graphite-monochromatized MoKα radiation (λ = 0.71073 Å) on a STOE IPDS II (Imaging Plate Diffraction System) at 190 K. The structure solutions and full-matrix least-square refinements based on F^2 were performed with SHELX-97 program package (38). Molecular diagrams were prepared by using the program Diamond 3.0. A dichroic green violet distorted rectangular thin plate with dimensions of 0.2 × 0.06 × 0.04 mm, M_r = 825.31, triclinic, space group P_1^- (No. 2), a = 6.477 (1), b = 9.411 (2), c = 18.504 (4) Å, α = 86.40 (3), β = 89.90 (3) γ = 85.15 (3), V = 2514 (3) Å^3, Z = 1, D_c = 1.222 g/cm^{-3}, μ = 0.591 mm^{-1} giving a final $R1$ value of 0.0609 for 293 parameters and 2,640 unique reflections with $I \geq 2\sigma(I)$ and $wR2$ of 0.1632 for all 7,817 reflections (R_{int} = 0.0567). A disorder has been modeled for the tertiary butyl group (C23–C26). CCDC-677194 contains the supplementary crystallographic data for this article. These data can be obtained free of charge at www.ccdc.cam.ac.uk/conts/retrieving.html (or from the Cambridge Crystallographic Data Centre, 12 Union Road, Cambridge CB2 1EZ, United Kingdom).

ACKNOWLEDGMENTS. We thank Harald Paulsen for co-supervising the diploma thesis of T.J. at the Johannes Gutenberg University of Mainz. This work was supported in part by the Deutsche Forschungsgemeinschaft (DFG) Center for Functional Nanostructures (CFN) at the Universität Karlsruhe (TH).

1. Blankenship RE (2002) *Molecular Mechanisms of Photosynthesis* (Blackwell, Oxford).
2. Blankenship RE, Matsuura K (2003) Light-harvesting antennas. *Light-Harvesting Antennas in Photosynthesis*, eds Green BR, Parson WW (Kluwer Academic Publishers, Dordrecht, The Netherlands), pp 195–217.
3. Balaban TS, Tamiaki H, Holzwarth AR (2005) Chlorins programmed for self-assembly. *Supramolecular Dye Chemistry*, Topics Current Chemistry 258, ed Würthner F (Springer, Berlin), pp 1–38.
4. Cohen-Bazire G, Pfennig N, Kunisawa R (1964) The fine structure of green bacteria. *J Cell Biol* 22:207–225.
5. Staehelin LA, Golecki JR, Fuller RC, Drews G (1978) Visualization of the supramolecular architecture of chlorosomes (Chlorobium type vesicles) in freeze-fractured cells of *Chloroflexus aurantiacus. Arch Mikrobiol* 119:269–277.
6. Staehelin LA, Golecki JR, Drews G (1980) Supramolecular organization of chlorosomes (chlorobium vesicles) and their membrane attachment sites in *Chlorobium limicola. Biochim Biophys Acta* 589:30–45.
7. Pšenčik J, *et al.* (2006) Internal structure of chlorosomes from brown-colored *Chlorobium* species and the role of carotenoids in their assembly. *Biophys J* 91:1433–1440.
8. Bryant DA, *et al.* (2007) Candidatus Chloracidobacterium thremophilum: An aerobic phototrophic acidobacterium. *Science* 317:523–526.
9. Manske AK, Glaeser J, Kuypers MMM, Overmann J (2005) Physiology and phylogeny of green sulfur bacteria forming a monospecific phototrophic assemblage at a depth of 100 meters in the Black Sea. *Appl Environ Microbiol* 71:8049–8060.
10. Beatty JT, *et al.* (2005) An obligatory photosynthetic bacterial anaerobe from a deep-sea hydrothermal vent. *Proc Natl Acad Sci USA* 102:9306–9310.
11. Oostergetel GT, *et al.* (2007) Long-range organization of bacteriochlorophyll in chlorosomes of Chlorobium tepidum investigated by cryo-electron microscopy. *FEBS Lett* 581:5435–5439.
12. Pšenčik J, *et al.* (2004) Lamellar organization of pigments in chlorosomes, the light harvesting complexes of green photosynthetic bacteria. *Biophys J* 87:1165–1172.
13. Holzwarth AR, Schaffner K (1994) On the structure of bacteriochlorophyll molecular aggregates in the chlorosomes of green bacteria. A molecular modelling study. *Photosynth Res* 41:225–233.
14. van Rossum B-J, *et al.* (2001) A refined model of the chlorosomal antennae of the green bacterium *Chorobium tepidum* from proton chemical shift constraints obtained with high-field 2-D and 3-D MAS NMR dipolar correlation spectroscopy. *Biochemistry* 40:1587–1595.
15. Kakitani Y, *et al.* (2006) Assembly of a mixture of isomeric BChl c from Chlorobium limicola as determined by intermolecular ^{13}C-^{13}C dipolar correlations: Coexistence of dimer-based and pseudo-monomer-based stackings. *Biochemistry* 45:7574–7585.
16. Egawa A, *et al.* (2007) Structure of the light-harvesting bacteriochlorophyll c assembly in chlorosomes from *Chlorobium limicola* determined by solid-state NMR. *Proc Natl Acad Sci USA* 104:790–795.
17. Linnanto JM, Korppi-Tommola JEI (2008) Investigation on chlorosomal antenna geometries: Tube, lamella and spiral-type self-aggregates. *Photosynth Res* 96:227–245.
18. Balaban TS, *et al.* (2003) Controlling chirality and optical properties of artificial antenna systems with self-assembling porphyrins. *Angew Chem Int Ed* 42:2190–2194.
19. Tamiaki H, Kimura S, Kimura T (2003) Self-aggregation of synthetic zinc 2^1-hydroxy-12^1/13^1-oxo-porphyrins. *Tetrahedron* 59:7423–7435.
20. Balaban TS, Linke-Schaetzel M, Bhise AD, Vanthuyne N, Roussel C (2004) Green self-assembling porphyrins and chlorins: Perfect mimics of the natural bacteriochlorophylls *c, d,* and *e. Eur J Org Chem* 3919–3930.
21. Balaban TS, *et al.* (2005) Structural characterization of artificial self-assembling porphyrins that mimic the natural chlorosomal bacteriochlorophylls *c, d* and *e. Chem Eur J* 11:2267–2275.
22. Balaban TS (2005) Tailoring porphyrins and chlorins for self-assembly in biomimetic artificial antenna systems. *Acc Chem Res* 38:612–623.
23. Linke-Schaetzel M, *et al.* (2004) Self-assembled chromophores for hybrid solar cells. *Thin Solid Films* 451–452c:16–21.
24. Huisjer A, *et al.* (2007) Photosensitization of TiO_2 and SnO_2 by artificial self-assembling mimics of the natural chlorosomal bacteriochlorophylls. *J Phys Chem C* 111:11726–11733.
25. Wakao N, *et al.* (1996) Discovery of natural photosynthesis using Zn-containing bacteriochlorophyll in an aerobic bacterium *Acidiphilium rubrum. Plant Cell Physiol* 37:889–893.
26. Steiner T (2002) The hydrogen bond in the solid state. *Angew Chem Int Ed* 41:48–76.
27. Chiefari J, *et al.* (1995) Models for the pigment organization in the chlorosomes of photosynthetic bacteria—Diastereoselective control of in-vitro bacteriochlorophyll c_S aggregation. *J Phys Chem* 99:1357–1365.
28. Ptaszek M, Yao Z, Savithri D, Boyle PD, Lindsey JS (2007) Synthesis and structural properties of porphyrin analogues of bacteriochlorophyll *c. Tetrahedron* 63:12629–12638.
29. Nozawa T, *et al.* (1994) Structures of chlorosomes and aggregated BChl c in *Chlorobium tepidum* from solid state high resolution CP/MAS ^{13}C NMR. *Photosynth Res* 41:211–223.
30. Balaban TS, Holzwarth AR, Schaffner K, Boender G-J, de Groot HJM (1995) CP-MAS ^{13}C-NMR Dipolar correlation spectroscopy of ^{13}C-enriched chlorosomes and isolated bacteriochlorophyll-c aggregates of. *Chlorobium tepidum*: The self-organization of pigments is the main structural feature of chlorosomes. *Biochemistry* 34:15259–15266.
31. van Rossum B-J, *et al.* (1998) Multidimensional CP-MAS ^{13}C-NMR of enriched chlorophyll. *Spectrochim Acta A* 54:1167–1176.
32. Ikonen TP, *et al.* (2007) X-ray scattering and electron cryomicroscopy study on the effect of carotenoid biosynthesis to the structure of *Chlorobium tepidum* chlorosomes. *Biophys J* 93:620–628.
33. Blankenship RE, *et al.* (1988) *Green Photosynthetic Bacteria*, Proc. EMBO Workshop, ed Olson JM (Plenum Press, New York), pp 57–68.
34. Brune DC, King GH, Blankenship RE (1988) *Photosynthetic Light-Harvesting Systems* (de Gruyter, Berlin), pp 141–151.
35. Balaban TS (2005) Relevance of the diastereotopic ligation of magnesium atoms of chlorophylls in the major light-harvesting complex II (LHC II) of green plants. *Photosynth Res* 86:251–262.
36. Savikhin S, *et al.* (1995) Ultrafast energy transfer in light-harvesting chlorosomes from the green sulphur bacterium *Chlorobium tepidum. Chem Phys* 194:245–258.
37. Lindsey JS, Woodford JN (1995) A simple method for preparing magnesium porphyrins. *Inorg Chem* 34:1063–1069.
38. Sheldrick GM (1997) SHELX-97. Program for X-ray Crystal Structure Determination and Refinement (Göttingen University, Germany).